

# Scaled Prototype of a Redundantly Fed, Gearless PMSM Wind Generator with Tooth Coil Winding and Solid Rotor Yoke

M. Sc. Nicolas Erd

Institute for Electrical Energy Conversion, TU Darmstadt, Darmstadt, Germany, nerd@ew.tu-darmstadt.de

Prof. Dr.-Ing. habil. Dr. h.c. Andreas Binder

Institute for Electrical Energy Conversion, TU Darmstadt, Darmstadt, Germany, abinder@ew.tu-darmstadt.de

## Abstract

Electromagnetical and thermal models are derived and the nominal operating point is analysed in both domains. The loss components that feed the thermal model are calculated from transient electromagnetic 2D-FEM simulation. The thermal model consists of two coupled 2D models: A 2D-FEM simulation for the stator and a thermal network for the rotor. Axial effects of the temperature distribution are discussed and analytically calculated.

## 1 Introduction

Large (> 1MW) gearless wind generators are equipped with outer rotor permanent magnet synchronous machines with solid rotor yoke [1, 2, 3]. Harmonic effects evoked by a tooth coil stator winding and redundancy operation cause significant eddy current losses in the solid rotor yoke leading to a decrease of overall efficiency and/or unacceptable local heating of the NdFeB-magnets [4, 5, 6]. Redundant feeding is defined here as the ability to continue operation in the case that one of the two feeding inverters is faulty. Operation is then continued by feeding only half of the machine's parallel branches by the still intact inverter and leaving the other branches idling. This operation will cause additional (sub-) harmonics of the stator field leading to rotor eddy current losses, which are depending on the spatial distribution of the fed winding segments on the circumference of the machine. A promising trade-off between high winding factor and acceptable rotor eddy current losses due to stator field harmonics is the two layer tooth coil winding with a number of slots per pole and phase  $q = 2/5$  [7, 24].

The concept of an outer rotor tooth coil wind generator with solid rotor yoke and redundant feeding is downsized to laboratory scale in order to proof feasibility. The scaled prototype is built in order to investigate the feasibility of tooth-coil winding and redundant feeding in combination with a solid rotor yoke, both leading to stator field harmonics causing rotor yoke eddy currents. This paper focusses on the electromagnetic and thermal simulation of the prototype machine.

## 2 Machine Data and Electromagnetic Model

The prototype machine is shown in Fig. 1 and the corresponding 2D-FEM model in Fig. 2. This model is used to calculate idling and nominal operation provided in Tab. 1. A fine mesh in the solid rotor yoke, as shown in Fig. 2, is necessary in order to calculate the eddy currents in the solid rotor yoke correctly. The main adaptations for downsizing are the following:

- Outer diameter (700 mm) limited by seamless pipe

- Air gap (2 mm) limited by manufacturing precision
- Semi closed slots in order to limit pulsation losses
- 40 poles in order to enable various feeding patterns in redundancy operation [8, 9, 24].

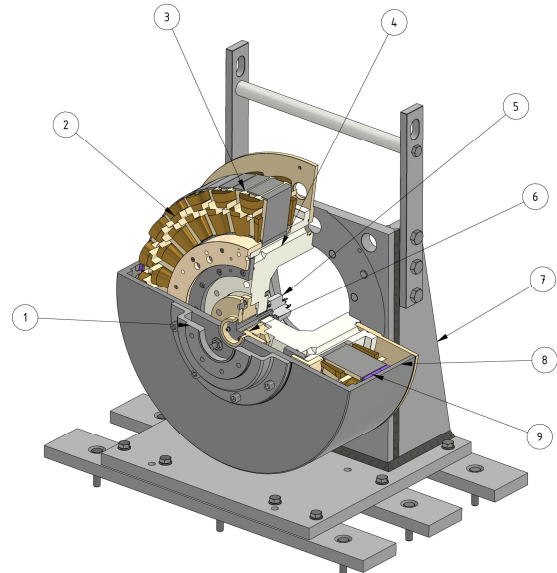


Fig. 1 3D-CAD-model (*Inventor* [17]) of the prototype machine; rotor in half-section; stator in three-quarter-section; A-side in front; B-side on the back: ① coupling flange; ② form-wound tooth-coil; ③ single tooth iron package; ④ stator support with internal water jacket; ⑤ incremental encoder; ⑥ bearing; ⑦ flange mount; ⑧ solid rotor yoke; ⑨ segmented magnets

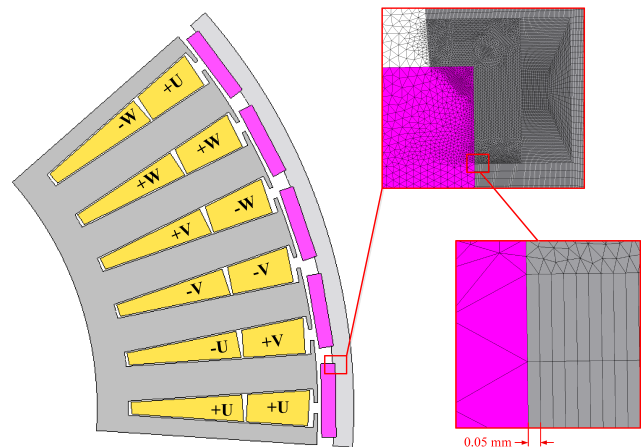


Fig. 2 2D-*MAG* [16] model of scaled prototype; tooth coil winding with  $q = 2/5$ ; rotor yoke skin mesh in two details

Tab. 1: FEM simulation results (*JMAG* 20.0 [16]) for prototype

	nominal op.	idling (gen.)
Number of slots per pole and ph. $q$	2/5	
Poles $2p$	40	
Axial stack length $l_{fe}$	90 mm	
Stator inner/outer diameter	400 mm / 658 mm	
Rotor yoke inner/outer diameter	679 mm / 700 mm	
Magnet height / air gap	8.5 mm / 2 mm	
Speed	60 min <sup>-1</sup>	60 min <sup>-1</sup>
Torque	2828 Nm	30.7 Nm
Mechanical power	17.77 kW	193 W
Stator frequency	20 Hz	20 Hz
Total losses	2895 W (100%)	193 W (100%)
AC-copper losses	2487 W (86%)	0 W (0%)
Stator iron losses	222.7 W (8%)	159 W (83%)
Eddy current loss: rotor magnets	40.1 W (1%)	11.6 W (6%)
Eddy current loss: rotor yoke	145.3 W (5%)	22.3 W (12%)
Stator fund. phase current $I_{s,1}$	35.01 A	0 A
Stator fund. phase voltage $U_{s,1}$	190.4 V	193.5 V
Generator efficiency	83.7 %	-
$\cos(\varphi_1)$	0.74 (ind.)	-

### 3 Thermal Model

Precise temperature calculation is key in the design process of an electrical machine. For the given prototype especially the following two thermal limits have to be fulfilled at all times: The winding insulation of class H has to be operated at or below 180°C hot-spot temperature and the rotor, more precisely the resin between permanent magnets and rotor yoke, has to be at or below 100°C. Further most losses are temperature dependent, therefore a reliable loss calculation relies on correct component temperatures. For the prototype the copper losses are dominant, therefore only these particular losses are modelled as temperature-dependent. Throughout the paper only stationary temperature distributions are concerned.

For the thermal calculation of electrical machines three approaches are widely-used [10]:

- i. Heat lumped parameter network
- ii. Numerical temperature calculation for solids
- iii. Computational fluid dynamics (CFD)

In the following these methods are discussed in the context of the given prototype.

#### 3.1 Stator Thermal FEM Model

The machine has an internal water jacket cooling and relatively large slots resulting in a significantly inhomogeneous temperature field in the winding over the cross section of the slot. But due to the relatively well known geometry, precise models for the stator can be derived.

In this particular case the numerical field calculation based on finite elements (FEM) for the stator is superior to classical lumped parameter networks in terms of mod-

elling effort and precision. Therefore the temperature field in the stator is calculated by a 2D, cross sectional, FEM model by the software *FEMM* [11] shown in Fig. 3. Since the model is 2D two major drawbacks follow: Firstly, only transversal heat flow is regarded, neglecting the heat flow along the wire due to relocation of the wire from turn to turn. And secondly, the model cannot predict the excess temperature in the winding overhang due to worse cooling conditions there. Both effects are discussed in section 3.3 and 3.4 respectively.

Utilizing basic symmetry considerations the 2D thermal model of the stator spans one slot pitch (Fig. 3) and has a depth of  $l_{fe}$ . The model consists from the inside to the outside of the following regions: The aluminium stator support contains the axial water cooling channels. On the boundary of the water channel a *Robin* condition models the convective heat transfer to the cooling water. The core region has a homogeneous volumetric loss density modelling the stator iron losses and a thermal coupling of the tooth tips for modelling convective heat transfer to the air gap, which is described in section 3.2. The slot region consists of four different sub-region types: Every single turn of the lower and upper layer coil is modelled by its blank cross section at its known position [25]. The pre-manufactured form wound coils slip onto the teeth and thereby leaving air pockets on the outer coil contour next to the neighbouring teeth, which are modelled by five air regions. The remaining slot area consists of the enamel and impregnation of the premanufactured coils and the impregnated slot liner. Both are modelled by homogenous substitutes, whose thermal conductivity is calculated from the different thermal conductivities weighted by the volume share. The complete stator AC-copper losses are modelled by a constant volumetric loss density over all bare conductors transferring losses generated in the winding overhang into the conductor sections embedded in the core. For both loss types in the stator (AC-copper losses and stator iron losses) all inhomogeneities are neglected.

In order to solve the problem the following input parameters are necessary: Average cooling agent temperature rise, heat transfer coefficient (HTC) in the cooling channel, iron losses, AC copper losses and the correction of volumetric loss density in the tooth tip accounting for the heat exchange between stator and rotor over the air gap as well as the correction of the copper losses due to heat exchange from winding overhang to inner air.

#### 3.2 Rotor Thermal Network and Coupling

The thermal network is derived from a longitudinal section of the prototype and assumes rotational symmetry. The total rotor losses  $P_r$ , which consist of eddy current losses in both rotor magnets and solid rotor yoke, are impressed in a single node in the rotor yoke (Fig. 4). The conductive heat resistances are calculated from basic formulas. The convective heat transfers from stator via air gap and from outer rotor surface to the ambient air are modelled by analytically calculated HTCs from principle geometries discussed in literature [12, 13, 14, 15, etc.] fol-

lowing the similarity principle of fluid dynamics. Alternatively more precise but numerically expensive CFD for accurate HTC calculation could be applied, which is outside the scope of this paper.

The thermal coupling of stator and rotor is implemented by an iterative calculation of heat exchange among stator tooth tip and rotor inner surface in the air gap  $\Delta P_{s,Fe}$  and heat exchange among stator winding overhang to inner air  $\Delta P_{s,Cu}$  according to the program sequence in Fig. 5: A start value for the heat exchange is assumed and the stator model (subscript A) is solved. The resulting temperatures of stator winding and tooth tip are used to calculate the heat exchanges by the rotor network (subscript B) applying the precalculated HTCs. The assumed heat exchanges are iteratively corrected according to the differences compared to the rotor model (subscript B).

### 3.3 Axial Heat Flow due to Repositioning of Conductors from Turn to Turn

The impact of heat flow along the wire is calculated by comparing the axial and transversal thermal resistances

$R_{th,ax}$  and  $R_{th,q}$  between two adjacent conductors of the winding (Fig. 6). A constant temperature difference of  $\Delta\theta$  is assumed between neighbouring conductors in every position. The thermal resistance in axial direction is calculated as (1) depending on the thermal conductivity of copper  $\lambda_{Cu}$ , the blank wire diameter  $d_{Cu}$  and the turn length  $l_{wdg}$ . The transversal heat resistance from conductor to neighbouring conductor is calculated for the geometry defined in Fig. 7 as  $R_{th,q}$  provided in (2). The problem is equivalent to the calculation of the electrical capacitance of a twin conductor [18, 19, 20]. The interspace between the conductors consisting of wire enamel, casting compound and air pockets is homogenized to an equivalent material, whose thermal conductivity  $\lambda_{iso}$  is calculated from the thermal conductivities of the aforementioned components weighted by their volume share as shown in Tab. 2. The provided formula (2) neglects the temperature drop in the copper, which is negligibly small compared to the temperature drop in the interspace due to  $\lambda_{Cu} \gg \lambda_{iso}$ . In summary, neglecting  $R_{th,ax}$  leads in this particular case to an insignificant overestimation of the thermal resistance.

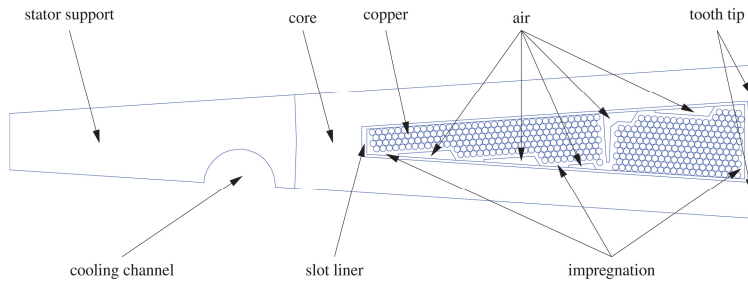


Fig. 3. Thermal stator model: 2D FEM (FEMM [11]); model spans one slot pitch

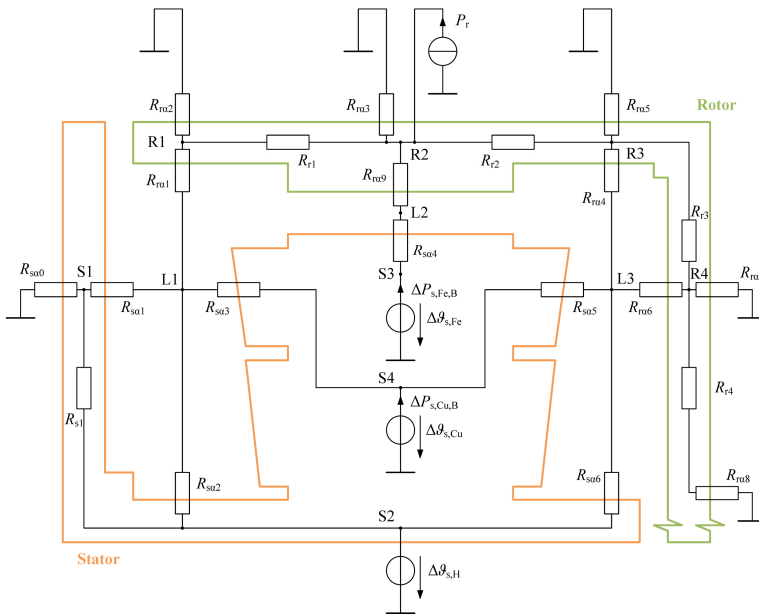


Fig. 4. Thermal rotor model: Lumped parameter thermal network; stator and rotor silhouette

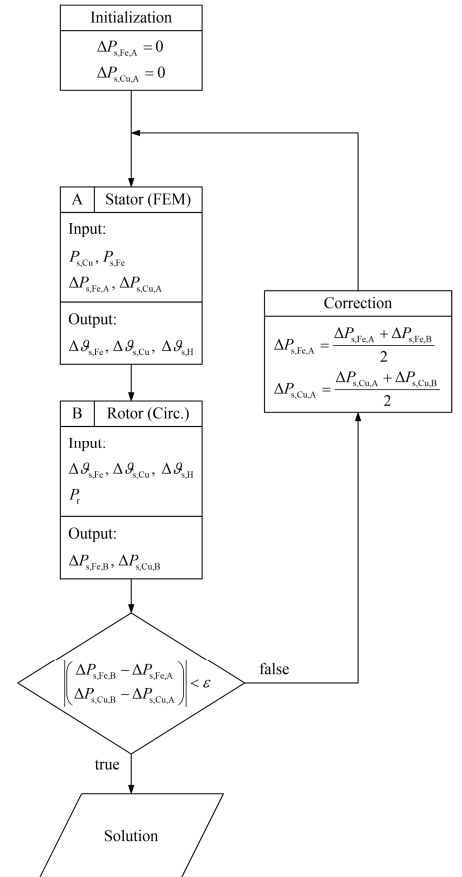


Fig. 5. Program sequence for calculation of heat exchange among stator and rotor

$$R_{th,ax} = \frac{l_{wdg}}{\lambda_{Cu} \cdot \frac{\pi}{4} \cdot d_{Cu}^2} = 325.5 \frac{K}{W} \quad (1)$$

$$R_{th,q} = \frac{1}{\pi \cdot \lambda_{iso} \cdot l_{wdg}} \cdot \ln \left( \frac{d_{Cu,o}}{d_{Cu}} + \sqrt{\left( \frac{d_{Cu,o}}{d_{Cu}} \right)^2 - 1} \right) = 0.85 \frac{K}{W} \quad (2)$$

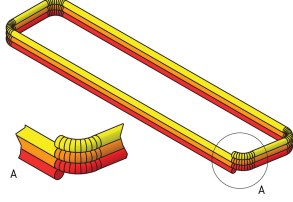


Fig. 6 Repositioning of conductor of an orthocyclic winding with three turns

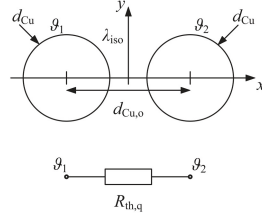


Fig. 7 Analytical model for calculation of equivalent transversal thermal resistance among adjacent conductors

Tab. 2: Properties of prefabricated form-wound coil

Parameter	Value
Blank copper diameter $d_{Cu}$	1.716 mm
Outer wire diameter $d_{Cu,o}$	1.800 mm
Turn length $l_{wdg}$	292.9 mm
Thermal conductivity copper $\lambda_{Cu}$	390 W/(m·K)
Thermal conductivity coil interspace $\lambda_{iso}$	0.40 W/(m·K)
Thermal conductivity enamel [21]	0.37 W/(m·K)
Thermal conductivity air	0.026 W/(m·K)
Thermal cond. casting compound [22]	0.5 W/(m·K)
Estimated casting compound fill factor	80%
Volume share enamel $A_{en}/A_{iso}$	7.0%
Volume share air $A_{air}/A_{iso}$	18.6%
Volume share casting compound $A_{cast}/A_{iso}$	74.4%

### 3.4 Excess Temperature Rise in the End Winding

The excess temperature in the end winding is calculated with a basic but reliable 1D bar model [23]. Accordingly all coils are summarized and described as a single axial bar with a homogeneous loss density but sectional lateral thermal resistance to ambience. For the given prototype two sections are used (see Fig. 8): The conductor length embedded in the indirectly water cooled iron core and the conductor length of the end winding. Due to symmetry the heat flux  $\Phi_{th}$  in the middle of the end winding and in the middle of the stator iron core are zero. The law of conservation of energy and *Fourier's* law lead to the ordinary differential equation (3). Therein  $r_{th,ax}$  is the specific longitudinal heat resistance (4),  $r_{th,q}$  is the specific transversal heat resistance to ambience (5), and  $p_L$  is the specific loss density (6). Conservatively no transversal heat dissipation is assumed in the end winding. In the stator core the specific transversal heat resistance is calculated from average copper temperature rise  $\Delta\vartheta_{Cu}$ , total copper losses  $P_{Cu}$  and iron stack length  $l_{fe}$ . Parameter values are provided in Tab. 3.

$$\frac{d^2 \Delta\vartheta(x)}{dx^2} - \frac{r_{th,ax}}{r_{th,q}} \cdot \Delta\vartheta(x) = -r_{th,ax} \cdot p_L \quad (3)$$

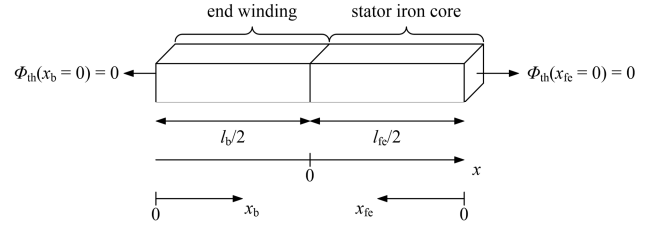


Fig. 8 Bar model for calculation of the axial temperature distribution in the winding; orientation of  $x$ -,  $x_b$ - and  $x_{fe}$ -coordinate

$$r_{th,ax} = \frac{1}{\lambda_{Cu} \cdot Q \cdot (N_{c,up} + N_{c,lw}) \cdot \frac{\pi}{4} \cdot d_{Cu}^2} \quad (4)$$

$$r_{th,q} = \begin{cases} r_{th,q,b} = \infty & x \leq 0 \quad (\text{end winding}) \\ r_{th,q,fe} = \frac{\Delta\vartheta_{Cu}}{P_{Cu}} \cdot l_{fe} & x > 0 \quad (\text{iron core}) \end{cases} \quad (5)$$

$$p_L = \frac{P_{Cu}}{l_b + l_{fe}} \quad (6)$$

The ODE is solved by (7)-(9) under consideration of continuity of temperature and heat flux.

$$\Delta\vartheta_b \left( 0 \leq x_b \leq \frac{l_b}{2} \right) = -\frac{r_{th,ax} \cdot p_L}{2} \cdot x_b^2 + c_1 \quad (7)$$

$$\Delta\vartheta_{fe} \left( 0 \leq x_{fe} \leq \frac{l_{fe}}{2} \right) = c_2 \cdot \cosh(\lambda \cdot x_{fe}) + r_{th,q,fe} \cdot p_L \quad (8)$$

$$\lambda = \sqrt{\frac{r_{th,ax}}{r_{th,q,fe}}} \quad c_2 = \frac{r_{th,ax} \cdot p_L \cdot l_b}{2 \cdot \lambda \cdot \sinh\left(\lambda \cdot \frac{l_b}{2}\right)} \quad (9)$$

$$c_1 = c_2 \cdot \cosh\left(\lambda \cdot \frac{l_b}{2}\right) + r_{th,q,fe} \cdot p_L + \frac{1}{8} \cdot r_{th,ax} \cdot p_L \cdot l_b^2$$

In Fig. 9 the distribution of temperature rise is shown for approximately the nominal point as described in Tab. 3. The maximum excess temperature of the winding overhang is 1.0 K and thereby negligible.

Tab. 3: Parameter for axial excess temperature calculation

Parameter	Value
Length end winding $l_b$	56 mm
Stator slots $Q$	48
Coil turns upper and lower coil $N_{c,up} / N_{c,lw}$	198 / 207
Copper losses $P_{Cu}$	2500 W
Avg. copper temperature rise $\Delta\vartheta_{Cu}$	90 K

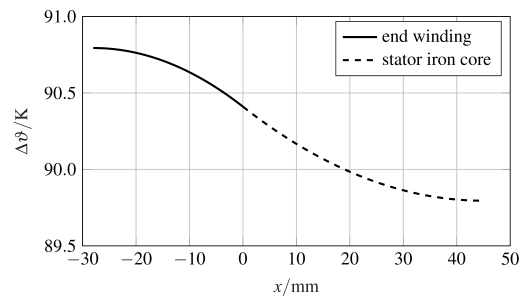


Fig. 9 Temperature distribution in winding over axial position in the  $x$ -coordinate system (see Fig. 8)

## 4 Simulation Results

The results of the thermal calculation of the nominal operation defined by Tab. 1 (column: nominal op.) are the temperature rise distribution in the stator shown in Fig. 10 and in the rotor. The latter and the heat exchange of rotor with stator and ambience are shown in Fig. 11.

Due to the deep slots an inhomogeneous temperature field occurs in the stator core as well as the stator winding. The quantitative numbers in Tab. 4 show, that the copper hot spot temperature rise exceeds the average copper temperature rise by 23 K. Therefore the thermal class 155 (F) will be exceeded and the machine utilizes class 180 (H) in nominal operation.

The calculation of the longitudinal network show a significant heat flux from stator to rotor of 248 W which is 1.33 times the amount of rotor losses. Nevertheless the rotor temperature rise of 40 K is not utilizing the thermal

limit of 100°C (magnet resin) at a max. ambient temperature of 40°C.

## 5 Conclusion

The derivation of a thermal model consisting of a 2D-FEM stator model coupled with a linear heat network was shown. A methodology was presented to check for axial effects which could possibly undermine this 2D-approach. Eventually the excess temperature rise of the end winding was checked.

For the nominal operating point the losses calculated from a transient electromagnetic FEM simulation were fed to the thermal models in order to calculate the temperature distribution. Apart from introducing the methodology, it was shown that the distribution of copper temperature rise is highly inhomogeneous and utilizes in nominal operation thermal class 180 (H) with a small reserve.

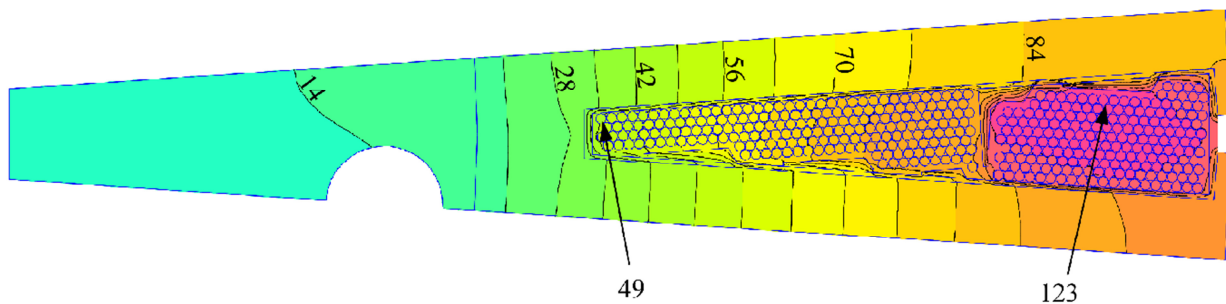
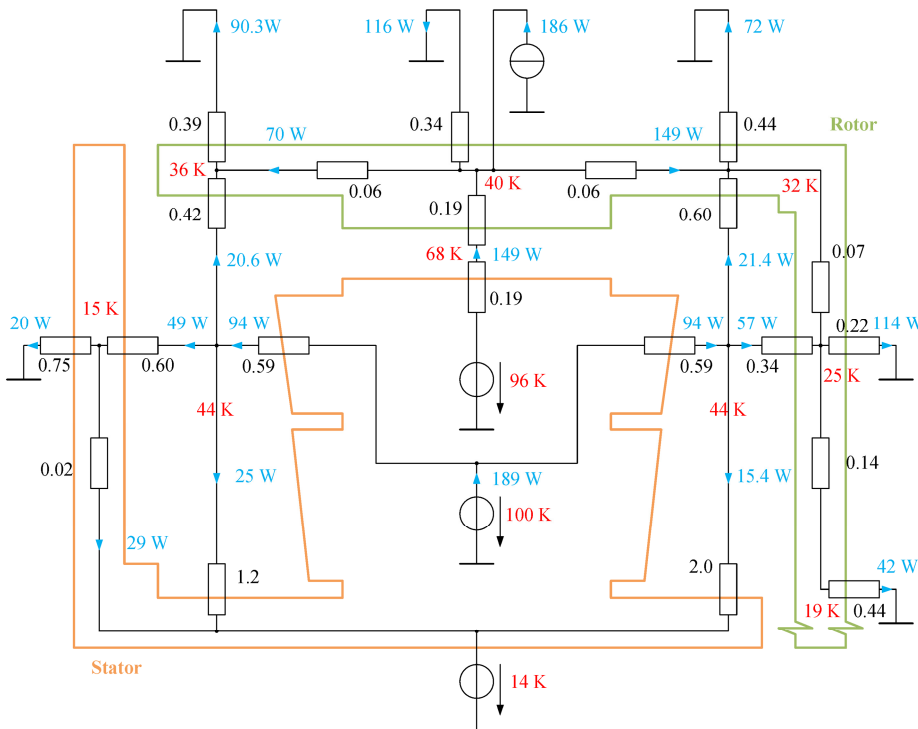


Fig. 10 Nominal operation: Simulated temp. rise distribution in the 2D stator FEM model (FEMM [11]); all values in K temperature rise over ambient temperature: labeled isothermal lines and min. /max. copper temp. rise by arrows



Tab. 4: Nominal Operation: Thermal calculation parameters and results according to Tab. 1

Parameter	Value
Ambient temp.	40°C
Avg. temp. rise coolant	7 K
HTC cooling channel	2282 W/(m <sup>2</sup> ·K)
Avg. copper temp. rise	100 K
Max. copper temp. rise	123 K
Min. copper temp. rise	49 K
Avg. stator core temp. rise	64 K
Tooth tip temp. rise	96 K
Avg. stator support temp. rise	14 K

Fig. 11 Nominal operation: Calculated heat exchange between stator and rotor and temperature rises; the thermal resistances are labeled with their thermal resistance in K/W.

## References

- [1] A. M. EL-Refaie, „Fractional-slot concentrated-windings synchronous permanent magnet machines: opportunities and challenges“, IEEE Trans. Ind. Electron. 57.1, pp. 107–121, Jan. 2010.
- [2] K. Reichert, „PM-Motors with concentrated, non overlapping windings, some characteristics“, in XVI Int. Conf. on Electrical Machines (ICEM), Cracow, Poland, Sep. 2004, p. 4.
- [3] V. Yaramasu, B. Wu, P. C. Sen, S. Kouro and M. Narimani, „High-power wind energy conversion systems: State-of-the-art and emerging technologies“, Proc. IEEE 103.5, pp. 740–788, May 2015.
- [4] H. Polinder, M. J. Hoeijmakers and M. Scuotto, „Eddy-current losses in the solid back-iron of permanent-magnet machines with concentrated fractional pitch windings“, in 3rd IET Int. Conf. on Power Electronics, Machines and Drives (PEMD), Antalya, Turkey, Apr. 2006, pp. 479–483.
- [5] A. Tassarolo, „A survey of state-of-the-art methods to compute rotor eddy-current losses in synchronous permanent magnet machines“, in IEEE Workshop on Electrical Machines Design, Control and Diagnosis (WEMDCD), Nottingham, UK, Apr. 2017, pp. 12–19.
- [6] G. Ugalde, Z. Q. Zhu, J. Poza and A. Gonzalez, „Analysis of rotor eddy current loss in fractional slot permanent magnet machine with solid rotor back-iron“, in XIX Int. Conf. on Electrical Machines (ICEM), Rome, Italy, Sep. 2010, pp. 1–6.
- [7] N. Erd and A. Binder, „Optimal design of gearless, permanent magnet wind generators with tooth coil winding and solid rotor yoke“ (in German: „Optimale Auslegung von getriebelosen, permanentmagneterregten Windgeneratoren mit Zahnspulenwicklung und massivem Rotorjoch“), Elektrotechnik und Informationstechnik 137.4–5, pp. 266–279, Aug. 2020.
- [8] N. Erd and A. Binder, „Numerical and analytical analysis of wave harmonics under spatially intermittent feeding“, in XXIII Int. Conf. on Electrical Machines (ICEM), Alexandroupolis, Greece, Sep. 2018, pp. 297–303.
- [9] N. Erd and A. Binder, „Eddy currents in solid rotor under spatially intermittent feeding of the stator winding“, in XXIII Int. Conf. on Electrical Machines (ICEM), Alexandroupolis, Greece, Sep. 2018, pp. 178–184.
- [10] A. Bolietti et al., „Evolution and modern approaches for thermal analyses of electrical machines“, IEEE Trans. on Ind. Electronics 56.3, Mar. 2009, pp. 871–882.
- [11] D. Meeker, „Finite Element Method Magnetics FEMM 4.2“, <https://www.femm.info>, visited: 22.06.2021
- [12] W. Benecke, „Temperature field and heat flow of small surface cooled AC motor with squirrel cage“ (in German: „Temperaturfeld und Wärmefluß bei kleineren oberflächengekühlten Drehstrommotoren mit Käfigläufer“, Elektrotechnische Zeitschrift ETZ-A 87.13, pp. 455–459, 1966.
- [13] J. Hak, „The air gap thermal resistance of electrical machines“ (in German: „Der Luftspalt-Wärmewiderstand einer elektrischen Maschine“), Archiv für Elektrotechnik 42.5, pp. 257–272, 1956.
- [14] W. Liebe, „Heat dissipation of electrical machines“ (in German: „Entwärmung Elektrischer Maschinen“), Hütte Elektrische Energietechnik - Maschinen, Springer, Berlin, pp. 280–299, 1978.
- [15] VDI-Wärmeatlas, 11 ed., Springer, 2013.
- [16] JSOL Corp., JMAG 20.0, Tokyo, Japan, <https://www.jmag-international.com>, visited: 22.06.2021
- [17] Autodesk Inc., Inventor 2020, San Rafael, USA, <http://www.autodesk.com>, visited: 22.06.2021
- [18] M. Filtz and H. Henke, „Exercises on electromagnetic fields“ (in German: „Übungsbuch Elektromagnetische Felder“), Springer, Berlin, 2007.
- [19] K. Küpfmüller et al., „Electromagnetical field calculation: An introduction“ (in German: „Theoretische Elektrotechnik: Eine Einführung“, ed. 19, Springer, Berlin, 2013.
- [20] O. Zinke and H. Brunswig, „Textbook on high-frequency engineering“ (in German: „Lehrbuch der Hochfrequenztechnik“), Springer, Berlin, 1965.
- [21] Solvay S.A., „Torlon: Technical Handbook“ (in German: „Torlon: Technisches Handbuch“, [https://www.solvayultrapolymers.com/zh/binaries/DPG\\_Torlon\\_Design\\_Guide\\_DE-204018.pdf](https://www.solvayultrapolymers.com/zh/binaries/DPG_Torlon_Design_Guide_DE-204018.pdf), visited: 22.06.2021
- [22] Elantas GmbH, Casting Compound MC 5430/W5868, [https://cdn.shopify.com/s/files/1/1250/8691/files/r\\_ep\\_5430.pdf?8949834880779206787](https://cdn.shopify.com/s/files/1/1250/8691/files/r_ep_5430.pdf?8949834880779206787), visited: 22.06.2021
- [23] J. Hak, „Inner axial heat resistance of an electrical machine“ (in German: „Die inneren axialen Wärmewiderstände einer elektrischen Maschine“, Archiv für Elektrotechnik 43.1, pp. 58–76, 1957.
- [24] N. Erd and A. Binder, „Concentrated Windings for Wind Generators with Solid Rotor Iron and Redundant Feeding“, XXIV. Int. Conf. on Electrical Machines (ICEM). Gothenburg, Sweden, Aug. 2020, pp. 2596–2602.
- [25] N. Erd and A. Binder, „Design and manufacturing of a high torque PMSM with tooth-coil winding and solid rotor yoke“, Electric Drives Production Conference (EDPC), Erlangen/Nuremberg, Germany, Dec. 2021, to be published.

## Authors



**Nicolas Erd** (born in 1989 in Berlin, Germany) received his B.Sc. and M.Sc. in Elect. Eng. from TU Berlin in 2013 and 2015. Since 2015 he is with the Institute of Electrical Energy Conversion at the TU Darmstadt as a research assistant concentrating on large PMSM for wind turbines.



**Andreas Binder** Senior Member IEEE, Member VDE, IET, VDI, EPE, received the degrees Dipl.-Ing. (diploma) and Dr. techn. (PhD) for Electrical Engineering from the University of Technology, Vienna/Austria, in 1981 and 1988. He worked in industry from 1981 to 1983 at ELIN Union AG, Vienna, on large synchronous generator design and from 1989 to 1997 as a group leader for developing DC and inverter-fed AC motors and drives at Siemens AG, Bad Neustadt and Erlangen, Germany. Since 1994 he is lecturer (habilitation) at University of Technology, Vienna/Austria, and since 1997 he is Head of the Institute of Electrical Energy Conversion, Darmstadt University of Technology, as a full professor. Research topics are high speed motors, permanent magnet E-Machines, bearing currents, drive technologies for hybrid and electric cars, drive systems for electric railways, magnetic suspension and magnetic bearings, generator systems e.g. for renewable energies.